Design of Linear-to-Circular Polarization Transformers Made of Long Densely Packed Metallic Helices

Mário G. Silveirinha, *Member, IEEE*

***Abstract*—In this work, we study the realization of realistic polarization transformers formed by long metallic helices. To this end, we propose a new homogenization model to characterize the propagation of electromagnetic waves in a medium formed by infinitely long helices. We derive approximate analytical expressions for the effective permittivity, effective permeability and the magnetoelectric tensor of the composite material, taking into account the effects of spatial dispersion. We apply the new homogenization model to characterize novel linear-to-circular polarization transformers. Our results show that the metamaterial screen may be designed in such a way that an incoming linearly polarized wave may be transformed into a circularly polarized transmitted wave, and that the transmission efficiency of such polarization transformer may be as high as 95%.**

***Index Terms*—Artificial materials, chiral media, homogenization, polarization transformers.**

I. INTRODUCTION

THE characterization and study of artificial materials is an important topic in modern electromagnetics. It has been suggested that properly designed microstructured materials may enable the realization of compact resonators, cavities, and waveguides that may surpass diffraction limits [1]–[3], and allow for the selective interaction of electromagnetic waves with objects or particles much smaller than the wavelength. Other interesting potentials of these microstructured materials include the realization of imaging devices with super-resolution [4]–[8], or squeezing electromagnetic waves through subwavelength narrow channels [9] with great electric field enhancement.

The objective of this work is to characterize the electromagnetic properties of an array of infinitely long helices, and investigate its possible application to the design of polarization transformation screens. Even though the study of artificial chiral media made of metallic helices is an old subject dating back to the beginning of the 20th century [10], [11], recently there has been a renewed interest in the properties of these composite materials after the proposal that a racemic mixture of canonical helices may yield an effective medium with negative parameters [12]. A related opportunity to obtain negative refraction using chiral materials was also identified in [13]. In this work we explore a different application of artificial chiral media, namely the possibility of designing a metamaterial screen to transform an incoming linear polarized wave into a circularly polarized wave.

It is well-known [11], [14], [15], that bi-isotropic chiral media have the ability to rotate the polarization state of an electromagnetic wave (gyrotropy), but that the ellipticity of the electric field (axis ratio of the polarization ellipse) remains unchanged. However, for certain applications at microwave and millimeter wave frequencies it may be interesting to transform the ellipticity of the incoming wave, rather than just to rotate its polarization state. Here, we propose a novel realistic metamaterial design of such polarization transformer using an array of very long densely packed metallic helices. Such material can be described as an anisotropic chiral material. The use of such materials for polarization transformation was reported in [11, p. 286].

In order to characterize the interaction of electromagnetic waves with the composite material, we apply the homogenization method proposed in [16] to derive an approximate analytical model for the dielectric function, taking into account spatial dispersion effects. It is proved that under some conditions the metamaterial can be described in terms of effective permittivity and permeability tensors and a magnetoelectric tensor which is a manifestation of the chiral effects. It is shown that the results predicted by our analytical model compare well with full wave band structure calculations, even when the helices are closely packed, or when the helix pitch is small. It is important to mention that in [17] a related spiral medium was homogenized using a local field theory. The main difference between our theory and the results presented in [17] is that our model describes a completely realistic physical structure, while in [17] the derived model is only approximate since the specific microstructure of the medium is partially ignored, and the spirals are modeled using an equivalent impedance. Due to this reason, the results of [17] are limited to the case in which the radius of the helices is much smaller than the lattice constant. In a different way, the solution derived here does not suffer from this inconvenience, and is valid even when the helices are closely packed. Only in this case a significant magnetoelectric coupling (which essential for the polarization-transformer application) may be induced.

We apply the derived homogenization model to characterize the reflection/transmission of waves by a finite slab of the metamaterial. Our study confirms that it may be possible to design the helices and tune the thickness of the metamaterial in such a

Manuscript received December 5, 2006; revised June 27, 2007. This work was supported by the Fundação para Ciência e a Tecnologia under project PDTC/EEA-TEL/71819/2006.

The author is with the Electrical Engineering Department, Instituto de Telecomunicações, Pólo II da Universidade de Coimbra, 3030 Coimbra, Portugal (e-mail: mario.silveirinha@co.it.pt).

Color versions of one or more of the figures in this paper are available online at http://ieeexplore.ieee.org.

Digital Object Identifier 10.1109/TAP.2007.915428

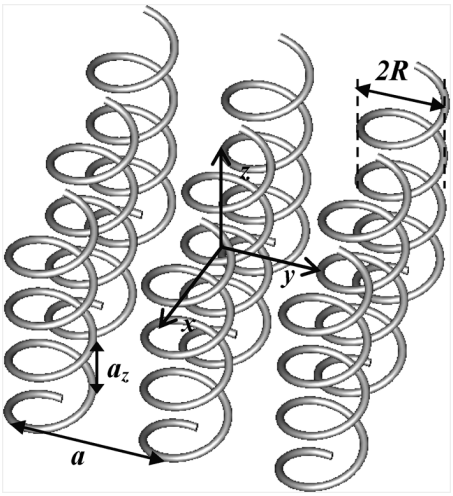

Fig. 1. Geometry of a periodic array of infinitely long PEC helices arranged in a square lattice.

way that a linearly polarized incoming wave is transformed into a wave with circular polarization. Moreover, it is shown that the efficiency of the proposed polarization transformer can be very high, with a reflection loss as small as 5%, and a good bandwidth.

This paper is organized as follows. In Section II we go over the homogenization method introduced in [16]. In Section III the homogenization method is used to extract the effective parameters of the metamaterial. In Section IV, the plane waves supported by the artificial medium are characterized. In Section V we use the new model to investigate the opportunity of designing polarization conversion screens. Finally, in Section VI the conclusion is drawn.

In this work, we assume that the fields are monochromatic and that the time dependence is $e^{j\omega t}$.

II. Geometry of the Material and Overview of the Homogenization Method

In this section, we present a brief overview of the homogenization procedure introduced in [16], and review the constitutive relations in spatially dispersive media.

A. Geometry

The metamaterial under study (Fig. 1) consists of a periodic array of infinitely long perfectly electrical conducting (PEC) helices. The helices are arranged into a square lattice, with lattice constant a, and stand in free-space. The parameterization of the axis of the helix inside the unit cell (one turn of the helix) is

$$\mathbf{r}_0(u) = \left(R\cos u, R\sin u, p\frac{u}{2\pi}\right), \quad -\pi < u < \pi \qquad (1)$$

where u is the parameterization variable, R is the radius of the helix, and $p > 0$ when the helix is right-handed and $p < 0$ when the helix is left-handed. The wire radius is r_w. The metamaterial is obtained by the periodic repetition of the unit cell defined by the primitive vectors $\mathbf{a}_1 = a\hat{\mathbf{u}}_x$, $\mathbf{a}_2 = a\hat{\mathbf{u}}_y$, and $\mathbf{a}_3 = a_z\hat{\mathbf{u}}_z$, as illustrated in Fig. 1. Note that the helix pitch is such that $a_z = |p|$. The helix surface ∂D is parameterized as detailed in Appendix A.

B. Calculation of the Nonlocal Dielectric Function

In a recent work [16], we introduced a completely general and systematic approach to homogenize arbitrary non-magnetic periodic materials. The method can fully characterize frequency dispersion, the magnetoelectric coupling (bianisotropic effects), and spatial dispersion of novel artificial media, even in frequency band-gaps or when the constituent materials are lossy. Instead of directly extracting the local parameters (permittivity, permeability, chirality, etc.) of the material, the method first calculates the nonlocal dielectric function $\overline{\overline{\varepsilon_{\rm eff}}} = \overline{\overline{\varepsilon_{\rm eff}}}(\omega, \mathbf{k})$ of the metamaterial. The local parameters—if meaningful—are extracted in a second step from the nonlocal dielectric function. This approach has several advantages, namely it is computationally simple and allows describing both local and nonlocal artificial materials in a unified manner. The constitutive relation implicit in the definition of the nonlocal dielectric function is

$$\mathbf{D}_g \equiv \varepsilon_0\mathbf{E}_{\rm av} + \mathbf{P}_g = \overline{\overline{\varepsilon_{\rm eff}}}(\omega, \mathbf{k}).\mathbf{E}_{\rm av} \qquad (2)$$

where $\mathbf{D}_g$ is the *generalized* electric displacement vector, $\mathbf{P}_g$ is the *generalized* polarization vector, and $\mathbf{E}_{\rm av}$ is the average electric field [16]. The constitutive relation only holds in the Fourier domain (i.e., it is assumed implicitly that the fields have been Fourier transformed in the space coordinates $\mathbf{r}$), and $\mathbf{k} = (k_x, k_y, k_z)$ represents the wave vector (the Fourier dual of $\mathbf{r}$). As discussed in [16], $\mathbf{P}_g$ can be written in terms of the classical polarization and magnetization vectors, and other higher order multipoles.

The main idea of the homogenization method is to calculate, for fixed $(\omega, \mathbf{k})$, the microscopic fields induced in the electromagnetic crystal when it is excited by an external Floquet-periodic electric current density of the form $\mathbf{J}_{\rm ext} = \mathbf{J}_{e,\rm av}e^{-j\mathbf{k}.\mathbf{r}}$, where $\mathbf{k}$ is the wave vector that defines the phase shift from cell to cell, and $\mathbf{J}_{e,\rm av}$ is a constant vector that defines the amplitude of the source (and indirectly the average macroscopic field $\mathbf{E}_{\rm av}$). Using the calculated microscopic fields, we can then characterize the generalized polarization vector $\mathbf{P}_g$, and afterwards it is possible to determine the dielectric function defined as in (2). For further details about the homogenization procedure the reader is referred to [16]. An important outcome of the theory presented in [16]—resulting from a method of moments (MoM) based solution of the problem—is that the dielectric function can be written in closed analytical form in terms of the expansion functions $\mathbf{w}_{n,\mathbf{k}}$ (of the induced microscopic currents) adopted in the MoM implementation. For the particular case in which the inclusions are metallic (PEC) it is proved in [16] that

$$\frac{\overline{\overline{\varepsilon_{\rm eff}}}}{\varepsilon_0}(\omega, \mathbf{k}) = \overline{\overline{\mathbf{I}}} + \frac{1}{\mathrm{V}_{\rm cell}}\sum_{m,n}\chi^{m,n}\int_{\partial D}\mathbf{w}_{m,\mathbf{k}}(\mathbf{r})e^{+j\mathbf{k}.\mathbf{r}}ds \otimes \int_{\partial D}\mathbf{w}_{n,-\mathbf{k}}(\mathbf{r})e^{-j\mathbf{k}.\mathbf{r}}ds \qquad (3a)$$

$$\chi_{m,n} = \int_{\partial D}\int_{\partial D} (\nabla_s.\mathbf{w}_{m,-\mathbf{k}}(\mathbf{r})\nabla'_s.\mathbf{w}_{n,\mathbf{k}}(\mathbf{r}') - \nabla_s.\mathbf{w}_{m,-\mathbf{k}}(\mathbf{r})\nabla'_s.\mathbf{w}_{n,\mathbf{k}}(\mathbf{r}')) \times \Phi_{p0}(\mathbf{r}|\mathbf{r}')dsds' \quad (3b)$$

where $\overline{\overline{\mathbf{I}}}$ is the identity dyadic, ∂D is the surface of the metallic inclusion in the unit cell, $\mathrm{V}_{\mathrm{cell}}$ is the volume of the unit cell, $\mathbf{w}_{n,\mathbf{k}}$ $(n = 1, 2, 3\ldots)$ form a complete set of tangential vector fields defined over ∂D (used for the expansion of the electric current density), $\nabla_s.$ stands for the surface divergence of a tangential vector field, $\beta = \omega\sqrt{\varepsilon_0\mu_0}$ is the free-space wave number, Φ_{p0} is a Green function, and the matrix $[\chi^{m,n}]$ is the inverse of $[\chi_{m,n}]$.

The Green function Φ_{p0} is defined in [16] and depends on both ω and $\mathbf{k}$. In this work, we assume that the long-wavelength limit approximation holds, i.e., that $\beta a \ll \pi$ and $|\mathbf{k}|a \ll \pi$. Using this hypothesis, it is possible to write

$$\Phi_{p0}(\mathbf{r}|\mathbf{r}';\omega,\mathbf{k}) \approx \Phi_{p0}(\mathbf{r}|\mathbf{r}';\omega=0,\mathbf{k}=0)e^{-j\mathbf{k}.(\mathbf{r}-\mathbf{r}')}. \quad (4)$$

Within such approximation, $\Phi_{p0}e^{+j\mathbf{k}.(\mathbf{r}-\mathbf{r}')}$ becomes independent of both frequency and wave vector. The Green function $\Phi_{p0}(\mathbf{r}|\mathbf{r}';\omega=0,\mathbf{k}=0)$ can be efficiently evaluated using the approach of [19].

III. Homogenization of the Artificial Medium

Next, the formalism presented in the previous section is used to homogenize the artificial material under study (Fig. 1). Instead of presenting a purely numerical answer, we will derive an approximate analytical solution. This has the advantage of giving important insights into the physics of the problem and into the application of the homogenization approach. Our strategy is to calculate first the dielectric function of the material (Sections III-A to III-D), and afterwards to extract the effective permittivity, permeability and the magnetoelectric tensors from $\overline{\overline{\varepsilon_{\mathrm{eff}}}}(\omega,\mathbf{k})$ (Section III-E).

A. The Expansion Functions

The first step to calculate the dielectric function $\overline{\overline{\varepsilon_{\mathrm{eff}}}}(\omega,\mathbf{k})$ given by (3) is to choose the expansion functions $\mathbf{w}_{n,\mathbf{k}}$. For simplicity, it is assumed that the radius r_w of the metallic wires is relatively thin: $r_w \ll a$ and $r_w \ll \lambda_0$ (thin-wire approximation; see Appendix A). Within this hypothesis, it is possible to consider that to a first approximation $\mathbf{J}_c$ flows along the helix axis [18]. Hence, the expansion functions of $\mathbf{J}_c$ may be taken equal to

$$\mathbf{w}_{n,\mathbf{k}}(\mathbf{r}) = \frac{1}{2\pi r_w}w_n(u)\mathbf{T}(u)e^{-j\mathbf{k}.\mathbf{r}} \quad (5)$$

where $\mathbf{T} = \mathbf{r}'_0/|\mathbf{r}'_0|$ is the unit vector tangent to the helix axis, $w_n(u)$ is a generic scalar function independent of $\mathbf{k}$ to be chosen ahead, and $\mathbf{r} = \mathbf{r}(u,\phi)$ is the parameterization of the helix surface given by (A1). As detailed in [16], the expansion functions $\mathbf{w}_n = \mathbf{w}_{n,\mathbf{k}}(\mathbf{r})$ must have the Floquet property. Thus (5) implies that the scalar expansion functions $w_n(u)$ are periodic functions of u with fundamental period 2π. A suitable set of expansion functions is the set of Fourier harmonics: $w_n(u) = \exp(jnu)$, $n = 0, \pm 1, \ldots$. For low frequencies it is expected that the induced current density $\mathbf{J}_c$ varies relatively slowly in one cell (see [18] for a related discussion). Hence, we expect that the behavior of the low frequency electromagnetic modes may be well described by only a few slowly varying expansion functions. Based on such physical considerations, in this work we will retain only (a linear combination of) the first 3 expansion functions. More specifically, we take the expansion functions equal to

$$w_1(u) = -\sin u; \quad w_2(u) = \cos u; \quad w_3(u) = 1. \quad (6)$$

This simplifying hypothesis will be validated later in the paper, by comparing the derived analytical model with full wave simulations.

For future reference, we note that when the expansion functions are of the form (5) the dielectric function given by (3) can be rewritten as

$$\frac{\overline{\overline{\varepsilon_{\mathrm{eff}}}}}{\varepsilon_h}(\omega,\mathbf{k}) = \overline{\overline{\mathbf{I}}} + \frac{1}{\mathrm{V}_{\mathrm{cell}}}\sum_{m,n}\chi^{m,n}\int w_m(u)\frac{d\mathbf{r}_0}{du}du \otimes \int w_n(u')\frac{d\mathbf{r}_0}{du'}du' \quad (7)$$

where $\mathrm{V}_{\mathrm{cell}} = a^2|p|$ is the volume of the unity cell. Using the results of Appendix A and (3), it is found that

$$\chi_{m,n} = \int\int dudu' \times \left[\left(\frac{dw_m}{du} + j\mathbf{k}.\frac{d\mathbf{r}_0}{du}w_m\right)\left(\frac{dw_n}{du'} - j\mathbf{k}.\frac{d\mathbf{r}_0}{du'}w_n\right) - \beta^2 w_m(u)w_n(u')\frac{d\mathbf{r}_0}{du}.\frac{d\mathbf{r}_0}{du'}\right]K_{p0}(u|u') \quad (8)$$

$$K_{p0}(u|u') = \frac{1}{(2\pi)^2}\int_0^{2\pi}\int_0^{2\pi} d\phi d\phi' \Phi_{p0}(\mathbf{r}|\mathbf{r}')e^{j\mathbf{k}.(\mathbf{r}-\mathbf{r}')}. \quad (9)$$

In (9), $\mathbf{r} = \mathbf{r}(u,\phi)$ and $\mathbf{r}' = \mathbf{r}(u',\phi')$ are defined as in (A1). Because of (4), the periodic thin-wire kernel defined above $K_{p0}(u|u')$ is independent of both frequency and wave vector.

B. Calculation of $\chi_{m,n}$

In order to obtain the effective permittivity using (7), next we calculate the elements $\chi_{m,n}$. Since $\chi_{m,n}(\mathbf{k}) = \chi_{n,m}(-\mathbf{k})$ it is sufficient to calculate $\chi_{m,n}$ for $n \geq m$. These elements can be written as linear combinations of integrals of the type

$$\int_{-\pi}^{\pi}\int_{-\pi}^{\pi} dudu' K_{p0}(u|u') \times \begin{Bmatrix}\sin(mu)\\ \cos(mu)\end{Bmatrix} \times \begin{Bmatrix}\sin(nu')\\ \cos(nu')\end{Bmatrix}, \quad m,n = 0,1,2. \quad (10)$$

All the above integrals are identically zero, except if the function associated with the primed and unprimed coordinates is the same. This property is proved in Appendix C. For convenience,

we introduce the following parameters (which only depend on the geometry of the artificial material):

$$C_m = \int_{-\pi}^{\pi}\int_{-\pi}^{\pi} dudu' \cos(mu)\cos(mu')K_{p0}(u|u'), m = 0,1,2 \tag{11a}$$

$$\tilde{C}_m = \int_{-\pi}^{\pi}\int_{-\pi}^{\pi} dudu' \sin(mu)\sin(mu')K_{p0}(u|u'), m = 1,2. \tag{11b}$$

The unities of C_m and $\tilde{C}_m$ are $[m^{-1}]$. It is proved in Appendix C that $C_1 = \tilde{C}_1$. Using the previous definitions and results, we obtain after straightforward calculations (the formulas are exact) that

$$\chi_{11} = C_1 + \left(\frac{R}{2}\right)^2 (C_0 + C_2)k_x^2 + \left(\frac{R}{2}\right)^2 \tilde{C}_2 k_y^2 + \left(\frac{p}{2\pi}\right)^2 C_1 k_z^2 - \beta^2 \left(\left(\frac{p}{2\pi}\right)^2 C_1 + \left(\frac{R}{2}\right)^2 (C_0 + C_2 + \tilde{C}_2)\right) \tag{12a}$$

$$\chi_{12} = j\frac{p}{2\pi} 2C_1 k_z + \left(\frac{R}{2}\right)^2 (C_0 + \tilde{C}_2 - C_2)k_x k_y \tag{12b}$$

$$\chi_{13} = jRC_1 k_y + R\frac{p}{2\pi}\left(C_1 + \frac{C_0}{2}\right) k_x k_z \tag{12c}$$

$$\chi_{23} = -jRC_1 k_x + R\frac{p}{2\pi}\left(C_1 + \frac{C_0}{2}\right) k_y k_z \tag{12d}$$

$$\chi_{33} = R^2 C_1 \left(k_x^2 + k_y^2\right) + \left(\frac{p}{2\pi}\right)^2 C_0 k_z^2 - \left(2R^2 C_1 + \left(\frac{p}{2\pi}\right)^2 C_0\right)\beta^2. \tag{12e}$$

Finally, χ_{22} is obtained from χ_{11} by interchanging the symbols k_x and k_y.

C. Calculation of $\chi^{m,n}$

Here, we calculate $[\chi^{m,n}]$, which is the inverse of the matrix $[\chi_{m,n}]$. These parameters can be written in closed analytical form, but the formulas are too cumbersome. To circumvent this problem, we use the long wavelength limit approximation to simplify the formulas.

In order to clarify the approach, let us consider for example the *exact* formula for χ^{11}

$$\chi^{11} = \frac{\chi_{22}\chi_{33} - \chi_{23}\chi_{32}}{\det(\chi)}. \tag{13}$$

Both the numerator and denominator of the above formula are polynomial functions of β, k_x, k_y and k_z. In our calculations only the lowest order terms in both the numerator and denominator were retained. Depending on the specific $\chi^{m,n}$ these terms are monomials of order one (sum of parcels involving β, k_x, etc.) or of order two (sum of parcels involving β^2, $k_x k_y$, βk_x, k_x^2, etc.). Within these approximations, it is found that

$$\det(\chi) \approx C_1^2\left[\left(\frac{p}{2\pi}\right)^2 C_0 k_z^2 - \left(2R^2 C_1 + \left(\frac{p}{2\pi}\right)^2 C_0\right)\beta^2\right] \tag{14a}$$

$$\chi^{11} \approx \frac{1}{C_1} + \frac{C_1^2 R^2 k_y^2}{\det(\chi)} \tag{14b}$$

$$\chi^{12} \approx -\frac{C_1^2 R^2 k_x k_y}{\det(\chi)} \tag{14c}$$

$$\chi^{13} \approx \frac{-jC_1^2 R k_y}{\det(\chi)} \tag{14d}$$

$$\chi^{23} \approx \frac{+jC_1^2 R k_x}{\det(\chi)} \tag{14e}$$

$$\chi^{33} \approx \frac{C_1^2}{\det(\chi)}. \tag{14f}$$

As before, χ^{22} is obtained from χ^{11} by interchanging the symbols k_x and k_y, and the remaining elements can be obtained using the relation $\chi^{m,n}(\mathbf{k}) = \chi^{n,m}(-\mathbf{k})$.

D. The Dielectric Function

To calculate $\overline{\overline{\varepsilon_{\text{eff}}}}$, it is noted that $\int w_n(u')(d\mathbf{r}_0/du')du'$ is equal to $\pi R\hat{\mathbf{u}}_x$, $\pi R\hat{\mathbf{u}}_y$, and $p\hat{\mathbf{u}}_z$, for n = 1,2,3, respectively. Hence, using (7) and (14) we obtain the desired dielectric function, shown in (15) at the bottom of the page, where $A = \pi R^2/p$ and

$$\varepsilon_t = 1 + \frac{(\pi R)^2}{\mathrm{V}_{\text{cell}}}\frac{1}{C_1} \tag{16}$$

$$\beta_{p1} = \sqrt{\frac{(2\pi p)^2}{C_0 p^2 \mathrm{V}_{\text{cell}} + 8C_1\pi^2 R^2 \mathrm{V}_{\text{cell}}}};$$

$$\beta_{p2} = \sqrt{\frac{(2\pi)^2}{C_0 \mathrm{V}_{\text{cell}}}}. \tag{17}$$

Note that $\overline{\overline{\varepsilon_{\text{eff}}}}$ is a function of frequency, wave vector, radius R, pitch of the helix p, and of A, β_{p1}, β_{p2} and ε_t, defined as above. The latter parameters are written exclusively in terms of C_0 and C_1, defined as in (11a). These two constants only depend on the geometry of the artificial material (but not on ω or $\mathbf{k}$), and are evaluated numerically. In Fig. 2, C_0 and C_1 are depicted as a function of the helix pitch for different R and r_w. It is also worth

$$\frac{\overline{\overline{\varepsilon_{\text{eff}}}}}{\varepsilon_0} = \begin{pmatrix} \varepsilon_t - \frac{A^2 k_y^2}{\beta^2/\beta_{p1}^2 - k_z^2/\beta_{p2}^2} & \frac{A^2 k_x k_y}{\beta^2/\beta_{p1}^2 - k_z^2/\beta_{p2}^2} & \frac{jAk_y}{\beta^2/\beta_{p1}^2 - k_z^2/\beta_{p2}^2} \\ \frac{A^2 k_x k_y}{\beta^2/\beta_{p1}^2 - k_z^2/\beta_{p2}^2} & \varepsilon_t - \frac{A^2 k_x^2}{\beta^2/\beta_{p1}^2 - k_z^2/\beta_{p2}^2} & \frac{-jAk_x}{\beta^2/\beta_{p1}^2 - k_z^2/\beta_{p2}^2} \\ \frac{-jAk_y}{\beta^2/\beta_{p1}^2 - k_z^2/\beta_{p2}^2} & \frac{jAk_x}{\beta^2/\beta_{p1}^2 - k_z^2/\beta_{p2}^2} & 1 - \frac{1}{\beta^2/\beta_{p1}^2 - k_z^2/\beta_{p2}^2} \end{pmatrix} \tag{15}$$

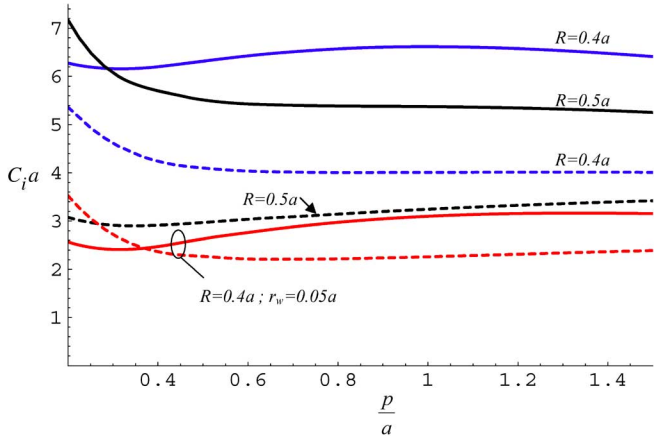

Fig. 2. Normalized constants C_0 (solid lines) and C_1 (dashed lines) as a function of the normalized helix pitch p and for different R. The radius of the wires is $r_w = 0.01a$ except on the curves where it is explicitly indicated that $r_w = 0.05a$.

noting that the geometrical parameter $A = \pi R^2/p$ is positive for right-handed helices, and negative for left-handed helices.

E. Bianisotropic Model

It is evident from (15) that the dielectric function depends explicitly on all components, k_x, k_y, and k_z of the wave vector. Indeed, our homogenization method is based on the constitutive relation (2), for which the effect of all microscopic currents is incorporated into the dielectric function, avoiding in this way the introduction of a permeability tensor and/or magnetoelectric coupling tensors. As discussed in [16], if the spatial dispersion is relatively weak, it may be possible to find local parameters $\overline{\overline{\varepsilon_r}}(\omega)$ and $\overline{\overline{\mu_r}}(\omega)$ (relative permittivity and permeability tensors), and (dimensionless) parameters that characterize the magnetoelectric coupling $\overline{\overline{\xi}}(\omega)$ and $\overline{\overline{\zeta}}(\omega)$, such that the artificial material is characterized by the classical bianisotropic constitutive relations [11]

$$\mathbf{D}_{\text{av}} = \varepsilon_0 \overline{\overline{\varepsilon_r}}.\mathbf{E}_{\text{av}} + \sqrt{\varepsilon_0\mu_0}\overline{\overline{\xi}}.\mathbf{H}_{\text{av}} \tag{18a}$$

$$\mathbf{B}_{\text{av}} = \sqrt{\varepsilon_0\mu_0}\overline{\overline{\zeta}}.\mathbf{E}_{\text{av}} + \mu_0\overline{\overline{\mu_r}}.\mathbf{H}_{\text{av}} \tag{18b}$$

where $\mathbf{B}_{\text{av}}$ is the macroscopic induction field, and $\mathbf{D}_{\text{av}} = \varepsilon_0\mathbf{E}_{\text{av}} + \mathbf{P}$ and $\mathbf{H}_{\text{av}} = \mathbf{B}_{\text{av}}/\mu_0 - \mathbf{M}$ are the classical electric displacement vector and magnetic field, respectively. It is simple to verify that in order that a material can be described by the local constitutive relations (18), it is necessary that

$$\frac{\overline{\overline{\varepsilon_{\text{eff}}}}}{\varepsilon_0}(\omega,\mathbf{k}) = \overline{\overline{\varepsilon_r}} - \overline{\overline{\xi}}.\overline{\overline{\mu_r}}^{-1}.\overline{\overline{\zeta}} + \left(\overline{\overline{\xi}}.\overline{\overline{\mu_r}}^{-1} \times \frac{\mathbf{k}}{\beta} - \frac{\mathbf{k}}{\beta} \times \overline{\overline{\mu_r}}^{-1}.\overline{\overline{\zeta}}\right) + \frac{\mathbf{k}}{\beta} \times \left(\overline{\overline{\mu_r}}^{-1} - \overline{\overline{\mathbf{I}}}\right) \times \frac{\mathbf{k}}{\beta}. \tag{19}$$

Thus, the material can be characterized by a local model only if $\overline{\overline{\varepsilon_{\text{eff}}}}$ is (at least approximately) a quadratic function of $\mathbf{k}$. In that case, the local parameters can be extracted from the dielectric function by expanding $\overline{\overline{\varepsilon_{\text{eff}}}} = \overline{\overline{\varepsilon_{\text{eff}}}}(\omega,\mathbf{k})$ in a Taylor series in $\mathbf{k}$ [16], [20].

The importance of the local model (18) relies on the fact that the effective parameters are independent of $\mathbf{k}$, and so the constitutive relations (18) are valid in the spatial domain. In particular, the classical boundary conditions (continuity of the tangential components of $\mathbf{E}$ and $\mathbf{H}$) can be used to solve boundary value problems involving interfaces with free-space [21]. Quite differently, for spatially dispersive materials the constitutive relations depend on the wave vector, and thus the boundary conditions at an interface may be very complicated to formulate, and additional boundary conditions may be required [21], [23].

Hence, the following question arises naturally: "is the model (15) equivalent to a bianisotropic model based on the constitutive relations (18)?" Or, in other words, "Can we find $\overline{\overline{\varepsilon_r}}$, $\overline{\overline{\mu_r}}$, and $\overline{\overline{\zeta}}$ such that to some approximation (19) is verified?"

Unfortunately, at least if we impose that $\overline{\overline{\varepsilon_r}}$, $\overline{\overline{\mu_r}}$, and $\overline{\overline{\zeta}}$ are independent of $\mathbf{k}$, the answer is negative. This can be easily verified by noting that $\overline{\overline{\varepsilon_{\text{eff}}}}$ is a function of $1/(\beta^2/\beta_{p1}^2 - k_z^2/\beta_{p2}^2)$, and consequently it is obvious that it cannot be expanded into a Taylor series around $k_z = 0$ and $\omega \approx 0$. Consequently, the artificial medium under-study is characterized by strong spatial dispersion.

Even though, it is not possible to obtain $\overline{\overline{\varepsilon_r}}$, $\overline{\overline{\mu_r}}$, and $\overline{\overline{\zeta}}$ independent of k_z such that to some approximation (19) holds, it is however possible to find parameters independent of k_x and k_y that verify (19). In fact, it can be confirmed by direct substitution that (19) is exactly verified for the following constitutive parameters:

$$\overline{\overline{\mu_r}} = \hat{\mathbf{u}}_x\hat{\mathbf{u}}_x + \hat{\mathbf{u}}_y\hat{\mathbf{u}}_y + \mu_{zz}\hat{\mathbf{u}}_z\hat{\mathbf{u}}_z$$

$$\mu_{zz} = \left(1 + \frac{\beta^2 A^2}{\beta^2/\beta_{p1}^2 - k_z^2/\beta_{p2}^2}\right)^{-1} \tag{20a}$$

$$\overline{\overline{\zeta}} = \zeta_{zz}\hat{\mathbf{u}}_z\hat{\mathbf{u}}_z = -\overline{\overline{\xi}}^t$$

$$\mu_{zz}^{-1}\zeta_{zz} = \frac{-j\beta A}{\beta^2/\beta_{p1}^2 - k_z^2/\beta_{p2}^2} \tag{20b}$$

$$\overline{\overline{\varepsilon_r}} = \varepsilon_t(\hat{\mathbf{u}}_x\hat{\mathbf{u}}_x + \hat{\mathbf{u}}_y\hat{\mathbf{u}}_y) + \varepsilon_{zz}\hat{\mathbf{u}}_z\hat{\mathbf{u}}_z$$

$$\varepsilon_{zz} = 1 - \frac{1}{\beta^2/\beta_{p1}^2 - k_z^2/\beta_{p2}^2} - \frac{\zeta_{zz}^2}{\mu_{zz}}. \tag{20c}$$

Is the bianisotropic model (20) useful? The dispersion characteristic for plane waves, $\omega = \omega(\mathbf{k})$, as well as the corresponding average electric and induction fields, $\mathbf{E}_{\text{av}}$ and $\mathbf{B}_{\text{av}}$, are exactly the same independently of the considered constitutive relations, i.e., independently of using (2) and (15) or using (18) and (20). Thus, from that point of view, the bianisotropic model (20) does not bring anything new. Indeed, as mentioned before, the importance of the bianisotropic model derives from the fact that in general only this model can be used to solve boundary value problems [21]. However, this is true only if the associated constitutive parameters $\overline{\overline{\varepsilon_r}}$, $\overline{\overline{\mu_r}}$, and $\overline{\overline{\zeta}}$ are independent of the wave vector $\mathbf{k}$, which is not the case here since (20) depends explicitly on k_z.

Nevertheless, since $\overline{\overline{\varepsilon_r}}$, $\overline{\overline{\mu_r}}$, and $\overline{\overline{\zeta}}$ depend exclusively on k_z (but not on k_x and k_y), they can still be used to impose the classical boundary conditions at an interface, provided the geometry of the problem is effectively two-dimensional (from a macroscopic point of view) and the z-direction is parallel to the interface between the metamaterial sample and free-space, e.g., if the metamaterial sample is an arbitrarily shaped cylinder oriented along the z-direction and the wave propagation is confined

to the xoy plane. In fact, in such circumstances, even though the helices are infinitely extended along the z-direction, their footprint in the xoy plane is electrically small for relatively long wavelengths. Thus, for on-plane propagation the metamaterial can be homogenized using *local parameters* (i.e., non-spatially dispersive parameters) given by (20). This result will be confirmed in Section V.

To give an idea of the variation with frequency of the effective parameters predicted by (20), in Fig. 3 we plot ε_{zz}, μ_{zz} and $\mathrm{Im}\{\zeta_{zz}\}$ (chirality), for on-plane propagation, i.e., $k_z = 0$ and for a material with $R = 0.4a$, $r_w = 0.01a$, $p = 0.5a$. It is seen that the effective permeability is less than one and is independent of frequency (within the accuracy of the proposed model). Similarly, the transverse effective permittivity (not shown) is $\varepsilon_t = 1.77$, and is also independent of frequency. On the other hand, the effective permittivity along z exhibits a Drude type variation. It is also seen that the chirality parameter has a resonant behavior near the static limit. For relatively low frequencies, the described results are qualitatively similar to those reported in [17].

IV. Properties of the Artificial Medium

The goal of this section is to characterize the plane wave solutions supported by the unbounded artificial material. First, it is useful to present a semi-heuristic discussion that gives some insights about the properties of the material under study. Thus, consider the case in which the radius of the helices R is vanishingly small, so that the artificial material reduces to the so-called "wire medium," formed by an array of parallel metallic wires oriented along the z-direction [22]. The wire medium supports three distinct types of electromagnetic modes: *i*) H-polarized modes for which $E_z = 0$ and $H_z \neq 0$; *ii*) E-polarized modes for which $E_z \neq 0$ and $H_z = 0$; and *iii*) transmission line modes for which both E_z and H_z vanish. It is well-known that for propagation in the xoy-plane and relatively large wavelengths the H-polarized waves propagate without interacting with the artificial medium, while the E-polarized waves are strongly attenuated.

Let us suppose that each metallic wire is slightly deformed into a helix, characterized by the radius R and the helix pitch p (see Fig. 1). How does this affect the electromagnetic modes in the artificial material? The main property of the modes that is changed is the polarization. In fact, it is well-known that when electromagnetic fields interact with chiral objects there may be a strong magnetoelectric coupling [11], [14]. Thus, the polarization of the perturbed electromagnetic modes may be no longer linear (as in the wire medium formed by straight wires), but may be elliptical. As in the regular wire medium, the perturbed E-polarized mode is still characterized by a cutoff plasma frequency. On the other hand, the H-polarized perturbed mode has no cutoff frequency and propagates for arbitrarily large wavelengths.

The electromagnetic modes supported by the metamaterial can be characterized more precisely using the derived homogenization model. The procedure to calculate the dispersion characteristic $\beta = \beta(\mathbf{k})$ and the polarization of the modes $\mathbf{E}_{\mathrm{av}}$ using the dielectric function $\overline{\overline{\varepsilon_{\mathrm{eff}}}}$ is well-known [16], [20]. It can be proven that the characteristic equation reduces to a polynomial of degree 3 in the variable β^2. Thus, for each wave vector $\mathbf{k}$ there are three different (positive) solutions for $\beta = \omega/c$, i.e., the homogenization model predicts that in the long wavelength limit three different modes may propagate in the metamaterial. Following our initial discussion, the electromagnetic modes can be thus classified as E-polarized perturbed modes, H-polarized perturbed modes, and transmission line perturbed modes. This situation contrasts sharply with the electrodynamics of common natural media, where only two independent modes are supported (i.e., only two distinct polarizations are allowed in common natural media). The emergence of the third electromagnetic mode in the artificial material is related to the strong spatial dispersion. This phenomenon occurs because the helical inclusions are infinitely long objects along the z-direction, and thus they cannot be considered electrically small, even near the static limit. This effect is well understood and studied for the case of straight metallic wires [18], [22], [23] and was also reported in [17].

It is useful to consider the particular case in which the wave travels in the xoy-plane (this is the situation of interest for the design of polarization transformers). For this configuration, supposing that $k_z = 0$, it can be proven that the dispersion characteristic of the modes is as in (21a) and (21b), shown at the bottom of the page, where $k_{||}^2 = \mathbf{k}_{||}.\mathbf{k}_{||}$ and $\mathbf{k}_{||} = (k_x, k_y, 0)$. The two solutions associated with (21a) correspond to the E-polarized mode ("+" sign is chosen in the equation) and to the H-polarized mode ("−" sign is chosen). From (21a) it is seen that, for on-plane propagation, the E-polarized perturbed wave is cutoff for $\beta < \beta_{p1}$. The solution (21b) is associated with transmission line modes, and corresponds to a collapsed band such that $\beta = 0$. In fact, for very low frequencies the transmission line modes propagate essentially along the wires, with dispersion characteristic $\beta \approx k_z/\sqrt{\varepsilon_t}$, and Poynting vector along the z-direction [22].

In order to check the accuracy of the proposed analytical model, we have calculated numerically the band structure of

$$\beta(k_{||},0) = \frac{1}{\sqrt{2\varepsilon_t}} \left\{ \left((1+\varepsilon_t)k_{||}^2 + \left(\varepsilon_t + A^2 k_{||}^2\right)\beta_{p1}^2\right) \pm \left[\left(-4\varepsilon_t k_{||}^2 \left(\beta_{p1}^2 + k_{||}^2 + A^2 k_{||}^2 \beta_{p1}^2\right)\right) + \left(\left((1+\varepsilon_t)k_{||}^2 + \left(\varepsilon_t + A^2 k_{||}^2\right)\beta_{p1}^2\right)\right)^2 \right]^{1/2} \right\}^{1/2} \tag{21a}$$

$$\beta(k_{||},0) = 0 \quad (\text{transmission line modes}) \tag{21b}$$

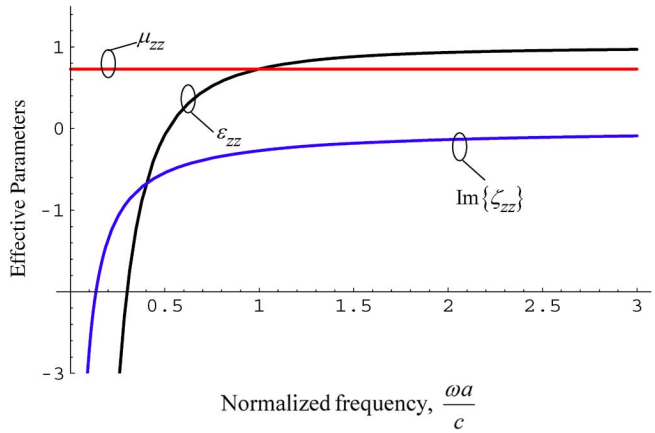

Fig. 3. Effective parameters ($k_z = 0$) for a material with $R = 0.4a$, $r_w = 0.01a$, $p = 0.5a$.

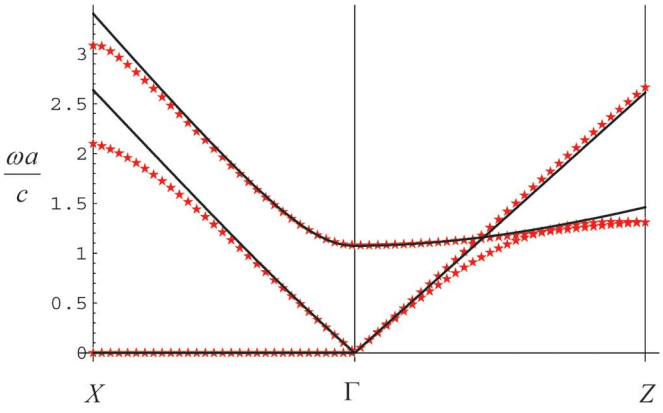

Fig. 4. Band structure for $R = 0.4a$, $r_w = 0.05a$, $p = 0.9a$ (only the first three bands are shown). Solid lines: analytical model; Star symbols: full wave numerical results. X, Γ and Z are highly symmetric points of the Brillouin zone.

the metamaterial using the full wave hybrid-plane-wave-integral-equation method proposed in [24]. To simplify the numerical implementation of the numerical method, it was assumed that the thin wire approximation holds, i.e., that the induced electric current flows along the direction tangent to the helical wires. Apart from this approximation, the full wave numerical results can be considered "exact." In Figs. 4 and 5, the results obtained using the analytical model (solid lines) are compared with the full wave band structure results (star symbols). The dispersion characteristic of the low-frequency eigen-waves is shown along the segments ΓX (propagation along the x-direction) and ΓZ (propagation along the z-direction) of the Brillouin zone (BZ) ($\mathbf{k}$-space). Note that by definition $\Gamma = (0,0,0)$, $X = (\pi/a, 0, 0)$, and $Z = (0, 0, \pi/|p|)$.

For propagation along the ΓX segment, with $\mathbf{k} = (k_x, 0, 0)$, the solid lines represent the solution given by (21). As seen, it compares very well with the full wave results, even for relatively large values of k_x (i.e., near the X point). Consistently with the initial heuristic discussion, it is seen in Fig. 4 that for low frequencies ($\beta a < \beta_{p1} a = 1.1$) the E-polarized perturbed mode is cutoff because it is strongly attenuated by the helical wires. As illustrated in Fig. 5, when the helix pitch is decreased to $p = 0.5a$ the cutoff wavenumber β_{p1} of the E-polarized perturbed mode also decreases. Similarly, it can be verified that the

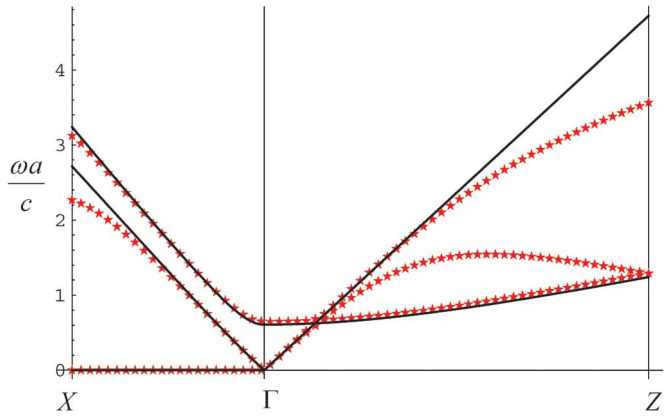

Fig. 5. Same as in Fig. 4 but for the parameters $R = 0.4a$, $r_w = 0.01a$, $p = 0.5a$.

cutoff frequency also decreases when the radius of the helix R increases (not shown). On the other hand, the dispersion characteristic $\beta = \beta(k)$ of the H-polarized perturbed mode is practically linear along the ΓX segment (near the origin of Brillouin zone), and has no cutoff for low frequencies.

For propagation along the ΓZ segment, with $\mathbf{k} = (0, 0, k_z)$, the situation is different. Indeed, the analytical model predicts that both the H-polarized and the transmission line perturbed modes are degenerate along z, and thus should propagate with the same phase velocity, independent of frequency. This is supported by the full wave results, but only for relatively low frequencies (roughly, $\beta a < 0.8$ in both figures). For higher frequencies, the full wave results show that the analytical model is not accurate since the dispersion characteristics of the two modes become clearly distinct. The lack of agreement is due to the several approximations made in Section III-C, and also because the number of expansion functions considered in the analytical model may be insufficient.

We have also characterized the polarization of the E- and H-perturbed modes, assuming propagation along the x-direction. Simple calculations demonstrate that the analytical model predicts that the polarization of the fields is proportional to

$$\mathbf{E}_{\mathrm{av}}(k_x) = jAk_x \frac{\beta_{p1}^2}{\beta^2}\hat{\mathbf{u}}_y + \left(\varepsilon_t - \frac{\beta_{p1}^2}{\beta^2}A^2 k_x^2 - \frac{k_x^2}{\beta^2}\right)\hat{\mathbf{u}}_z \qquad k_y = k_z = 0. \quad (22)$$

The above result is valid for both the E- and H-polarized perturbed modes (however, from (21a) it is clear that for each family of modes the relation between β and k_x is different). Provided k_x is a real number (i.e., for propagating modes) the wave is thus transverse electromagnetic (TEM) with elliptic polarization, being the principal axes of the polarization ellipse along the y- and z-directions. Moreover, it can be easily verified that the H-perturbed mode has left-handed polarization if the helices are right-handed ($p > 0$, or equivalently $A > 0$), and has right-handed polarization if the helices are left-handed ($p < 0$). Conversely, the polarization of the E-perturbed mode has the same handiness as the helices (provided it is a propagating

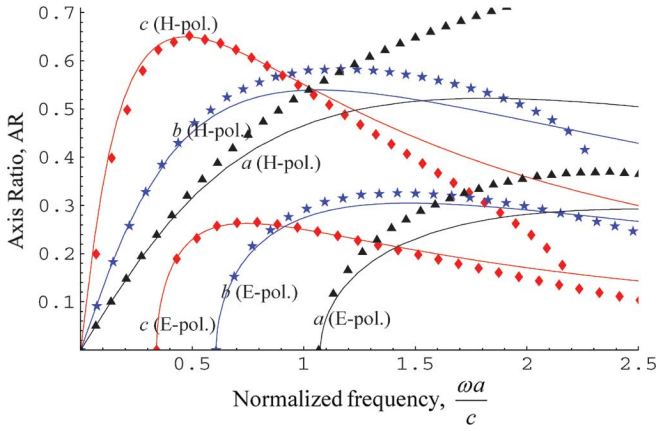

Fig. 6. Axis ratio of the E-polarized and H-polarized electromagnetic modes as function of the normalized frequency (propagation along the x-direction is implicit). Solid lines: Analytical model; Diamond/Triangle/Star symbols: Full wave results. The radius of the helices is $R = 0.4a$. The wire radius and the helix pitch are: (a) $r_w = 0.05a, p = 0.9a$, (b) $r_w = 0.01a, p = 0.5a$, (c) $r_w = 0.01a, p = 0.2a$.

mode with k_x a real number). Thus, the E- and H- polarized perturbed modes rotate in opposite directions. Finally, it can be verified that when the E-polarized mode is cutoff ($\beta < \beta_{p1}$) the polarization of the wave is linear.

In order to validate the theory, we have numerically calculated the polarization of the electromagnetic modes. To this end, the electromagnetic modes are obtained numerically and the electric field is then averaged over the unit cell [24]. The comparison between the full wave results (discrete symbols) and (22) (solid lines) is depicted in Fig. 6, where the axis ratio of the polarization ellipse is plotted as a function of the normalized frequency for different metamaterial configurations. It is seen that the general agreement is good, even though the helices are closely packed ($R = 0.4a$) and the helix pitch can be as small as $p = 0.2a$ (curve c). For convenience we defined the axis ratio (AR) of the polarization ellipse as the ratio between the minor axis of the ellipse and the major axis of the ellipse, and so $AR \leq 1$ (usually AR is defined as the inverse of this quantity).

From Fig. 6, it is apparent that the AR of the H-polarized perturbed mode is maximal near the plasma frequency where the E-polarized perturbed mode starts propagating. The results suggest that by properly designing the inclusions it may be possible to fabricate a metamaterial screen such that at some frequency the E-polarized perturbed mode is cutoff, whereas the H-polarized perturbed mode propagates with circular polarization ($AR = 1$). In such conditions, if a linearly polarized plane wave impinges on the metamaterial screen (with polarization in the xoy plane) it can only transfer power to the eigenmode with circular polarization.

V. Polarization Transformers

In what follows we study the possibility of using the magnetoelectric coupling intrinsic to the helical inclusions to design a linear-to-circular polarization transformer.

A. Propagation Along the x-Direction

In order to characterize the fields scattered by a slab of the metallic helices, it is necessary to study the properties of the electromagnetic modes with further detail for the case of propagation along the x-direction.

For a given (normalized) frequency $\beta = \omega/c$, the E- and H-polarized perturbed modes propagate along the x-direction with propagation constant k_x^E and k_x^H, respectively. Using (21a), it can be verified that

$$k_x^{(H,E)} = \frac{1}{\sqrt{2+2A^2\beta_{p1}^2}} \times \left\{\beta^2\left(1+A^2\beta_{p1}^2+\varepsilon_t\right)-\beta_{p1}^2 \pm \left[4\beta^2\left(\beta_{p1}^2-\beta^2\right)\left(1+A^2\beta_{p1}^2\right)\varepsilon_t + \left(\beta^2\left(1+A^2\beta_{p1}^2+\varepsilon_t\right)-\beta_{p1}^2\right)^2\right]^{1/2}\right\}^{1/2} \quad (23)$$

where the "+" sign is chosen is chosen for the H-perturbed modes and the "−" sign is chosen for the E-perturbed modes.

As discussed in Section IV, the average electric field of the modes is given by (22). On the other hand, the corresponding average induction field verifies $\eta_0(\mathbf{B}_{\rm av}/\mu_0) = (\mathbf{k}/\beta) \times \mathbf{E}_{\rm av}$ ($\eta_0 = \sqrt{\mu_0/\varepsilon_0}$ is the impedance of free-space), and so we have that

$$\eta_0\frac{\mathbf{B}_{\rm av}}{\mu_0} = -\left(\varepsilon_t - \frac{\beta_{p1}^2}{\beta^2}A^2k_x^2 - \frac{k_x^2}{\beta^2}\right)\frac{k_x}{\beta}\hat{\mathbf{u}}_y + jAk_x\frac{\beta_{p1}^2}{\beta^2}\frac{k_x}{\beta}\hat{\mathbf{u}}_z. \quad (24)$$

From (18b) the macroscopic magnetic field is given by

$$\eta_0\mathbf{H}_{\rm av} = \overline{\overline{\mu_r}}^{-1}.\eta_0\frac{\mathbf{B}_{\rm av}}{\mu_0} - \overline{\overline{\mu_r}}^{-1}.\overline{\overline{\zeta}}.\mathbf{E}_{\rm av}. \quad (25)$$

Substituting (22) and (24) in the above, it follows that:

$$\eta_0\mathbf{H}_{\rm av}(k_x) = -\left(\varepsilon_t - \frac{\beta_{p1}^2}{\beta^2}A^2k_x^2 - \frac{k_x^2}{\beta^2}\right)\frac{k_x}{\beta}\hat{\mathbf{u}}_y + \left(j\frac{Ak_x}{\mu_{zz}}\frac{\beta_{p1}^2}{\beta^2}\frac{k_x}{\beta} - \frac{\zeta_{zz}}{\mu_{zz}}\left(\varepsilon_t - \frac{\beta_{p1}^2}{\beta^2}A^2k_x^2 - \frac{k_x^2}{\beta^2}\right)\right)\hat{\mathbf{u}}_z \quad (26)$$

where μ_{zz} and ζ_{zz} are given by (20).

B. Scattering Problem

Next, we apply the analytical model to characterize the scattering of plane waves by a finite slab of the metamaterial. The slab is assumed infinite and periodic along the y-direction (the lattice constant is a), and has N_L layers of helices arranged along the x-direction. Thus the equivalent thickness of the slab is $L = N_L a$. The geometry for the case $N_L = 2$ is depicted in the inset of Fig. 7. The interfaces with free-space are taken equal to $x = 0$ and $x = L$. The helices are centered at $(a/2 + na, ma, 0)$, with m integer and $n = 0, 1, \ldots N_L - 1$.

The incident wave propagates along the x-direction (normal incidence) and is polarized along the y-direction, $\mathbf{E}^{\rm inc} = E^{\rm inc}e^{-jk_x^{\rm inc}x}\hat{\mathbf{u}}_y$, where $k_x^{\rm inc} \equiv \beta$ is the propagation

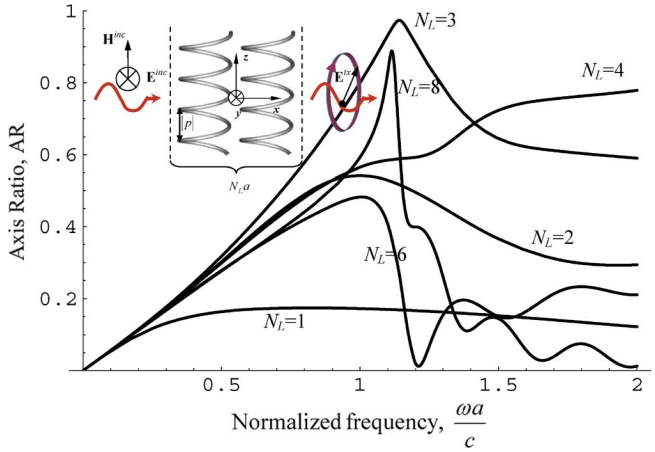

Fig. 7. Axis ratio of the transmitted wave as function of the normalized frequency varying the number of layers N_L of the metamaterial screen. The radius of the helices is $R = 0.4a$, the wire radius is $r_w = 0.05a$, and the helix pitch is $p = 0.9a$. The inset shows the geometry of the problem for the case $N_L = 2$ layers.

constant of the incoming wave. The total electromagnetic fields for $x < 0$ are given by

$$\mathbf{E} = E^{\text{inc}} e^{-jk_x^{\text{inc}} x}\hat{\mathbf{u}}_y + E^{\text{inc}}(\rho_{co}\hat{\mathbf{u}}_y + \rho_{cr}\hat{\mathbf{u}}_z)e^{+jk_x^{\text{inc}} x} \quad (27a)$$

$$\eta_0\mathbf{H} = E^{\text{inc}} e^{-jk_x^{\text{inc}} x}\hat{\mathbf{u}}_z + E^{\text{inc}}(\rho_{cr}\hat{\mathbf{u}}_y - \rho_{co}\hat{\mathbf{u}}_z)e^{+jk_x^{\text{inc}} x},\ x < 0 \quad (27b)$$

where ρ_{co} is the reflection coefficient for the co-polarized wave, and ρ_{cr} is the reflection coefficient for the cross-polarized wave. Similarly, for $x > L$, the transmitted fields are of the form

$$\mathbf{E} = E^{\text{inc}}(t_{co}\hat{\mathbf{u}}_y + t_{cr}\hat{\mathbf{u}}_z)e^{-jk_x^{\text{inc}} x} \quad (28a)$$

$$\eta_0\mathbf{H} = E^{\text{inc}}(-t_{cr}\hat{\mathbf{u}}_y + t_{co}\hat{\mathbf{u}}_z)e^{-jk_x^{\text{inc}} x},\quad x > L \quad (28b)$$

where t_{co} is the transmission coefficient for the co-polarized wave, and t_{cr} is the transmission coefficient for the cross-polarized wave.

Inside the metamaterial slab, $0 < x < L$, the fields can be written in terms of E- and H-polarized perturbed modes predicted by the homogenization model (the transmission line modes cannot be excited for normal incidence). Hence, we have the expansions

$$\mathbf{E} = c_E^+\mathbf{E}_{\text{av}}(k_x^E)e^{-jk_x^E x} + c_E^-\mathbf{E}_{\text{av}}(-k_x^E)e^{+jk_x^E x} + c_H^+\mathbf{E}_{\text{av}}(k_x^H)e^{-jk_x^H x} + c_H^-\mathbf{E}_{\text{av}}(-k_x^H)e^{+jk_x^H x} \quad (29a)$$

$$\mathbf{H} = c_E^+\mathbf{H}_{\text{av}}(k_x^E)e^{-jk_x^E x} + c_E^-\mathbf{H}_{\text{av}}(-k_x^E)e^{+jk_x^E x} + c_H^+\mathbf{H}_{\text{av}}(k_x^H)e^{-jk_x^H x} + c_H^-\mathbf{H}_{\text{av}}(-k_x^H)e^{+jk_x^H x} \quad (29b)$$

where $\mathbf{E}_{\text{av}}(k_x)$, $k_x^{(E,H)}$, and $\mathbf{H}_{\text{av}}(k_x)$ are defined by (22), (23), and (26), respectively, and $c_{E,H}^{\pm}$ are the unknown amplitudes of the excited modes.

In order to determine the reflection coefficients ρ_{co} and ρ_{cr}, the transmission coefficients t_{co} and t_{cr}, and the four coefficients $c_{E,H}^{\pm}$, we need to impose that the tangential electromagnetic fields (E_y, E_z, H_y, H_z) are continuous at the interfaces $x = 0$ and $x = L$. In this way, we obtain an 8×8 linear system that can be solved numerically with respect to the unknowns.

C. Design of Polarization Transformers

It is manifest from (29) that when an incoming wave illuminates the metamaterial screen it may excite both the E- and H- polarized perturbed modes. It is expected that for $\beta < \beta_{p1}$, when the E-perturbed mode is cutoff, an incoming wave (with electric field in the xoy plane) will couple most of its energy to the H-perturbed wave, and consequently the metamaterial screen may behave as a very efficient polarization transformer.

It is appropriate to mention that the design of polarization transformers exploiting the anisotropy and chirality of materials was also studied in [11, p. 286]. It was found that for a fixed frequency the maximal change in the ellipticity of a plane wave as it propagates in an unbounded anisotropic chiral material is achieved at a distance $L = \pi/(k_x^H - k_x^E)$ (in our notations) from a given reference plane [11, p. 290]. The previous formula can be regarded as rough estimation of the required metamaterial thickness (this condition alone does not guarantee the desired linear to circular polarization conversion). It implies that to design a thin polarization transformer it is necessary that $k_x^H - k_x^E$ is as large as possible (the formula assumes that both propagation constants are real; this may not be the case in our problem). From Fig. 4 (for example), it is seen that $k_x^H - k_x^E$ is maximum at the plasma frequency $\beta = \beta_{p1}$, when $k_x^E = 0$. This suggests that to design a thin polarization transformer one should operate the metamaterial around the plasma frequency $\beta = \beta_{p1}$.

To have a more precise idea of the suggested possibilities we solved numerically the scattering problem formulated in Section V-B, using the homogenization model. We computed the AR of the transmitted wave as a function of frequency for a screen with $R = 0.4a$, $r_w = 0.05a$, and $p = 0.9a$. The result is depicted in Fig. 7 for different number of layers of helices N_L. It is seen that the AR of the transmitted wave depends considerably on the thickness of the screen. This is understandable because by varying N_L we may enhance or deteriorate the AR of the transmitted wave due to the interference between the different modes excited in the metamaterial slab. Moreover, the AR of the transmitted wave may be much larger than the AR of the H-polarized perturbed mode (Fig. 6). Consistently with our previous discussion and the results of Fig. 6, the peak of the AR is attained at $\beta \approx \beta_{p1}$, which for this example corresponds to $\beta_{p1}a \approx 1.1$. It is noticeable that for $N_L = 3$ layers and $\beta \approx \beta_{p1}$ the axis ratio of the polarization ellipse is $AR \approx 1$, i.e., for these parameters the desired polarization transformation is achieved.

In order to validate the results suggested by Fig. 7 (obtained using homogenization theory), the periodic method of moments (MoM) was used to calculate the AR of the transmitted wave. The corresponding full wave numerical results (discrete symbols) are depicted in Figs. 8 and 9 superimposed on the analytical model results (solid lines), for different metamaterial geometries. The figures reveal that despite the helices being closely packed $(R = 0.4a)$ and the helix pitch being as small as $p = 0.2a$ (Fig. 9), the agreement between the analytical model and the full wave results is very good. The slight disagreement for high frequencies is related to the fact that the granularity of

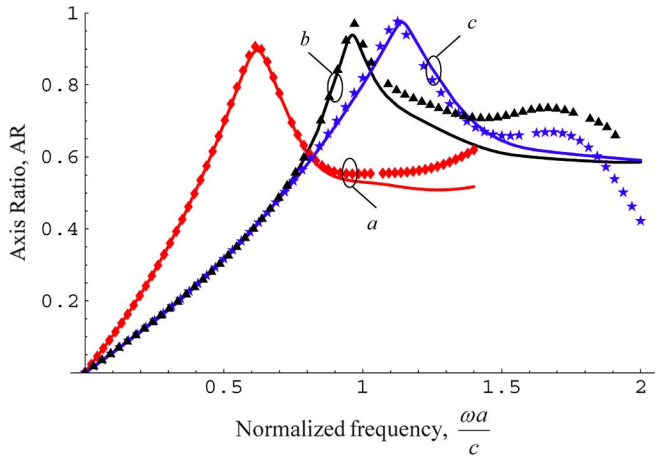

Fig. 8. Axis ratio of the transmitted wave as function of the normalized frequency. Solid lines: Analytical model; Diamond/Triangle/Star symbols: Full wave results. The radius of the helices is $R = 0.4a$. The wire radius, helix pitch, and the number of layers are: (a) $r_w = 0.01a, p = 0.5a, N_L = 5$, (b) $r_w = 0.01a, p = 0.9a, N_L = 5$, (c) $r_w = 0.05a, p = 0.9a, N_L = 3$.

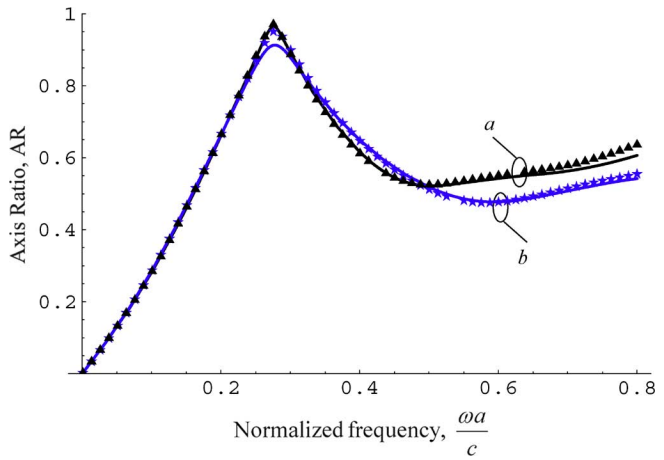

Fig. 9. Axis ratio of the transmitted wave as function of the normalized frequency. Solid lines: Analytical model; Triangle/Star symbols: Full wave results. The radius of the helices is $R = 0.4a$ and the helix pitch is $p = 0.2a$. The wire radius, and the number of layers are: (a) $r_w = 0.01a, N_L = 8$ and (b) $r_w = 0.05a, N_L = 6$.

the artificial material cannot be neglected when the lattice constant becomes a significant fraction of the wavelength. In all the examples, we have chosen the minimum value for N_L that ensures that the AR of the transmitted wave is close to unity at some frequency (in general $\beta \approx \beta_{p1}$).

The numerical results confirm that the incoming linear wave can indeed be transformed into a circularly polarized wave. Notice that in the examples considered here $p > 0$ (the helices are right-handed) and, consequently, the polarization of the transmitted wave is left-handed (see Section IV). Figs. 8 and 9 suggest that by decreasing the helix pitch p, the $AR = 1$ condition occurs at a smaller normalized frequency. However, the number of layers N_L necessary to obtain the polarization conversion increases.

An important parameter to characterize the efficiency of the polarization conversion is the fraction of transmitted power,

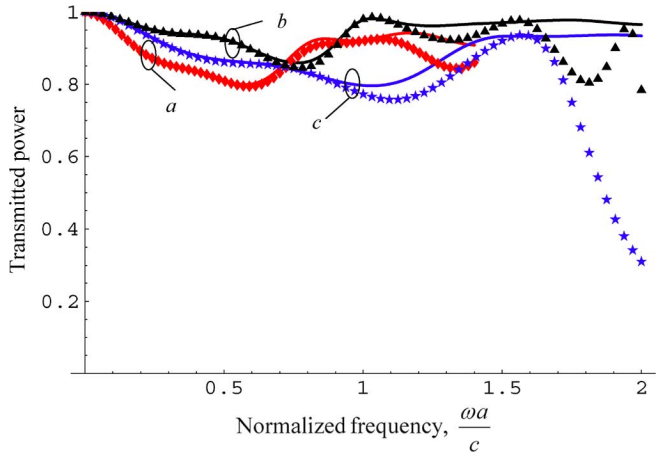

Fig. 10. Fraction of the transmitted power as a function of the normalized frequency. Solid lines: Analytical model; Diamond/Triangle/Star symbols: Full wave results. The parameters for curves a, b and c are as in Fig. 8.

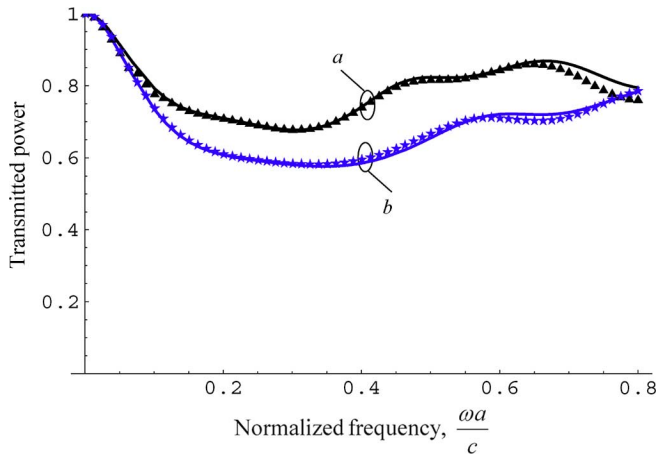

Fig. 11. Fraction of the transmitted power as a function of the normalized frequency. Solid lines: Analytical model; Triangle/Star symbols: Full wave results. The parameters for curves a, and b are as in Fig. 9.

given by $T = 1 - |\rho_{co}|^2 - |\rho_{cr}|^2$, where ρ_{co} is the reflection coefficient for the co-polarized wave, and ρ_{cr} is the reflection coefficient for the cross-polarized wave [see (27)]. We calculated T as a function of the normalized frequency using both the analytical model of Section V-B and the periodic MoM. The results associated with Figs. 8 and 9 are depicted in Figs. 10 and 11, respectively, and confirm the very good agreement between the homogenization results (solid lines) and the full wave results (discrete symbols).

It is seen that for some of the geometries the transmission efficiency can be nearly 100% at the frequency of interest (in particular this true for curve b in Fig. 10, which corresponds to $r_w = 0.01a, p = 0.9a, N_L = 5$). The results of Fig. 11 indicate that the transmission efficiency may deteriorate if the helix pitch is too small, even though a transmission as high as 70% is still possible at the frequency where $AR \approx 1$. The results presented here clearly demonstrate the potentials of the proposed metamaterial screens as polarization transformers, and prove their robustness both in terms of frequency response and transmission efficiency.

VI. Conclusion

In this work, we studied the realization of polarization transformers using realistic microstructured materials. To this end, we developed a new homogenization model to characterize a periodic medium formed by long metallic helices, and extracted its effective permittivity, permeability and chirality. The proposed analytical model was compared with full wave band structure simulations showing good agreement, even for demanding cases where the helices are densely packed and the pitch is relatively small. It was shown that the proposed metamaterial may act effectively as a linear-to-circular polarization transformer, with low reflection loss, good bandwidth, and yielding a transmitted wave with axis ratio very close to one. The theoretical results are supported by full wave simulations.

Appendix A

Here, we present the details about the mathematical model of the helices. The parameterization of the surface of a generic helix is

$$\mathbf{r}(u,\phi) = \mathbf{r}_0(u) + r_w\left(\cos\phi\mathbf{N}(u) + \sin\phi\mathbf{B}(u)\right),\ \ 0 < \phi < 2\pi \tag{A1}$$

where r_w is the wire radius, $\mathbf{r}_0(u)$ is a parameterization of the helix axis given by (1), and $\mathbf{N}$ and $\mathbf{B}$ are the associated normal and binormal vectors [25]. The tangent vector is $\mathbf{T} = \mathbf{r}_0'/|\mathbf{r}_0'|$. It can be proven that provided the curvature $K = R/(R^2 + (p/2\pi)^2)$ and the torsion $\tau = (p/2\pi)/(R^2 + (p/2\pi)^2)$ of the helix satisfy $Kr_w \ll 1$ and $\tau r_w \ll 1$ (thin wire approximation) then the density of surface current $\mathbf{J}_c$ is of the form (a similar property holds for the expansion functions $\mathbf{w}_n$)

$$\mathbf{J}_c \approx \frac{I(u)}{2\pi r_w}\mathbf{T} \tag{A2}$$

where $I(u)$ is the current along the wires. The infinitesimal area of a surface element is $ds = \sqrt{g}du\,d\phi$, where $\sqrt{g} \approx r_w|\mathbf{r}_0'|$. The surface divergence of $\mathbf{J}_c$ verifies

$$\nabla_S.\mathbf{J}_c = \frac{1}{\sqrt{g}}\frac{1}{2\pi}\frac{dI}{du}. \tag{A3}$$

Appendix B

In this Appendix, we present some relevant properties of $K_{p0}(u|u')$, the periodic thin wire periodic kernel defined by (9), with $\mathbf{r}(u,\phi)$ given by (A1). The approximation (4) is used, and to keep the notation short we define $\hat{\Phi}_{p0}(\mathbf{r}|\mathbf{r}') = \Phi_{p0}(\mathbf{r}|\mathbf{r}')e^{+j\mathbf{k}.(\mathbf{r}-\mathbf{r}')}$.

Property 1:

$$K_{p0}(u|u') = K_{p0}(u'|u) \tag{B1}$$

This property is a consequence of $\hat{\Phi}_{p0}(\mathbf{r}|\mathbf{r}') = \hat{\Phi}_{p0}(\mathbf{r}'|\mathbf{r})$.

Property 2: Suppose that the wire parameterisation verifies $\mathbf{r}_0(u+T) = \mathbf{r}_0(u) + \mathbf{a}$ for arbitrary u, where $\mathbf{a}$ is a primitive vector of the lattice (eventually zero) and T is a constant. Then

$$K_{p0}(u|u') = K_{p0}(u+T|u') = K_{p0}(u|u'+T). \tag{B2}$$

In fact, $\mathbf{r}_0(u+T) = \mathbf{r}_0(u) + \mathbf{a}$ implies that $\mathbf{r}(u+T,\phi) = \mathbf{r}(u,\phi) + \mathbf{a}$, and since $\hat{\Phi}_{p0}(\mathbf{r}) = \hat{\Phi}_{p0}(\mathbf{r}+\mathbf{a})$ the property is obvious.

Property 3: Let R be a rotation by 90° in the horizontal plane: $R:(x,y,z) \to (-y,x,z)$. Suppose that the wire parameterisation satisfies $\mathbf{r}_0(u+u_0) = R.\mathbf{r}_0(u) + \mathbf{v}$ for arbitrary u, where $\mathbf{v}$ is a constant vector. It is also assumed that the lattice is orthorhombic and that the transversal lattice is a square lattice. In that case, we have

$$K_{p0}(u|u') = K_{p0}(u+u_0|u'+u_0). \tag{B3}$$

In fact, $\mathbf{r}_0(u+u_0) = R.\mathbf{r}_0(u) + \mathbf{v}$ implies that $\mathbf{r}(u+u_0,\phi) = R.\mathbf{r}(u,\phi) + \mathbf{v}$. Due to the lattice symmetry we also have that $\hat{\Phi}_{p0}(\mathbf{r}) = \hat{\Phi}_{p0}(R.\mathbf{r})$ and thus, $\hat{\Phi}_{p0}(\mathbf{r}|\mathbf{r}'|) = \hat{\Phi}_{p0}(R.\mathbf{r}+\mathbf{v}|R.\mathbf{r}'+\mathbf{v})$. Using the previous formulas we readily obtain the desired result.

Property 4: Let τ be a reflection relatively to one of the coordinate axis (e.g., $\tau_x:(x,y,z) \to (-x,y,z)$). Suppose that the wire axis satisfies $\mathbf{r}_0(-u) = -\tau.\mathbf{r}_0(u)$ for arbitrary u, and that the lattice is orthorhombic. In that case, we have

$$K_{p0}(u|u') = K_{p0}(-u|-u'). \tag{B4}$$

Indeed, $\mathbf{r}_0(-u) = -\tau.\mathbf{r}_0(u)$ implies that $\mathbf{r}(-u,-\phi) = -\tau.\mathbf{r}(u,\phi)$. Since the lattice is orthorhombic we also have that $\hat{\Phi}_{p0}(\mathbf{r}) = \hat{\Phi}_{p0}(-\tau.\mathbf{r})$. Substituting these formulas into (9) we readily obtain (B4).

Appendix C

Here we prove some useful properties of the integrals given by (10). To begin with, we prove

$$\int_{-\pi}^{\pi}\int_{-\pi}^{\pi} dudu' K_{p0}(u|u')\cos(mu)\sin(nu') = 0. \tag{C1}$$

Indeed, since the helix satisfies $\mathbf{r}_0(-u) = -\tau_x.\mathbf{r}_0(u)$, we can apply property (B4) and after changing the integration variables we easily obtain (C1). Note that because of (B1) we can interchange the roles of $\sin$ and $\cos$ in the above expression.

On the other hand, we have

$$\begin{aligned}\int_{-\pi}^{\pi}\int_{-\pi}^{\pi} dudu' K_{p0}(u|u')e^{jmu}e^{jnu'} &= \int_{-\pi}^{\pi}\int_{-\pi}^{\pi} dudu' K_{p0}\left(u+\frac{\pi}{2}\middle|u'+\frac{\pi}{2}\right)e^{jmu}e^{jnu'} \\ &= (-j)^{m+n}\int_{-\pi}^{\pi}\int_{-\pi}^{\pi} dudu' K_{p0}(u|u')e^{jmu}e^{jnu'}\end{aligned} \tag{C2}$$

where the first identity is a consequence of (B3) with $u_0 = \pi/2$, and the second identity is a consequence of (B2) and of the fact that the integrations are over one period $T = 2\pi$. From the previous result, the following is obvious:

$$\int_{-\pi}^{\pi}\int_{-\pi}^{\pi} dudu' K_{p0}(u|u') e^{jmu} e^{jnu'} = 0, \quad \text{if } m+n \text{ is not multiple of } 4. \quad \text{(C3)}$$

In particular, extracting the real part of the above expression and using the fact that $K_{p0}(u|u')$ is real, it follows that (assuming from now on that if $m+n$ is not multiple of 4):

$$\int_{-\pi}^{\pi}\int_{-\pi}^{\pi} dudu' K_{p0}(u|u') \cos(mu)\cos(nu') = \int_{-\pi}^{\pi}\int_{-\pi}^{\pi} dudu' K_{p0}(u|u') \sin(mu)\sin(nu'). \quad \text{(C4)}$$

Putting $m = n = 1$, we find that, $C_1 = \tilde{C}_1$. On the other hand, replacing n by $-n$ in (C4) and summing term by term the resulting identity with (C4), we obtain

$$\int_{-\pi}^{\pi}\int_{-\pi}^{\pi} dudu' K_{p0}(u|u') \cos(mu)\cos(nu') = \int_{-\pi}^{\pi}\int_{-\pi}^{\pi} dudu' K_{p0}(u|u') \sin(mu)\sin(nu') = 0 \quad \text{(C5)}$$

when both $m+n$ and $m-n$ are not multiples of 4. In particular, the above identity holds for $m \neq n$ and $0 \leq m, n \leq 2$.

REFERENCES

[1] N. Engheta, "An idea for thin, subwavelength cavity resonators using metamaterials with negative permittivity and permeability," *IEEE Antennas Wireless Propag. Lett.*, vol. 1, p. 10, 2002.

[2] A. Alù and N. Engheta, "Optical nano-transmission lines: Synthesis of planar left-handed metamaterials in the infrared and visible regimes," *J. Opt. Soc. Am. B*, vol. 23, no. 3, pp. 571–583, 2006.

[3] F. Falcone, T. Lopetegi, J. D. Baena, R. Marqués, F. Martín, and M. Sorolla, "Effective negative- ε stop-band microstrip lines based on complementary split ring resonators," *IEEE Microw. Wireless Compon. Lett.*, vol. 14, pp. 280–282, June 2004.

[4] J. B. Pendry, "Negative refraction makes a perfect lens," *Phys. Rev. Lett.*, vol. 85, p. 3966, 2000.

[5] A. Grbic and G. V. Eleftheriades, "Overcoming the diffraction limit with a planar left handed transmission line lens," *Phys. Rev. Lett.*, vol. 92, p. 117403, Mar. 2004.

[6] P. A. Belov, Y. Hao, and S. Sudhakaran, "Subwavelength microwave imaging using an array of parallel conducting wires as a lens," *Phys. Rev. B*, vol. 73, p. 033108 (1–4), 2006.

[7] C. Luo, S. G. Johnson, J. D. Joannopoulos, and J. Pendry, "Subwavelength imaging in photonic crystals," *Phys. Rev. B*, vol. 68, p. 045115 (1–15), 2003.

[8] M. G. Silveirinha, P. A. Belov, and C. Simovski, "Subwavelength imaging at infrared frequencies using an array of metallic nanorods," *Phys. Rev. B*, vol. 75, p. 035108 (1–12), 2007.

[9] M. Silveirinha and N. Engheta, "Tunneling of electromagnetic energy through sub-wavelength channels and bends using near-zero-epsilon materials," *Phys. Rev. Lett.*, vol. 97, p. 157403, 2006.

[10] K. F. Lindmann, *Annalen der Physik*, vol. 63, pp. 621–644, 1920.

[11] I. V. Lindell, A. H. Sihvola, S. A. Tretyakov, and A. Viitanen, *Electromagnetic Waves in Chiral and Bi-Isotropic Media*. Norwood, MA: Artech House, 1994.

[12] S. A. Tretyakov, *Analytical Modeling in Applied Electromagnetics*. Norwood, MA: Artech House, 2003, p. 253.

[13] J. B. Pendry, "A chiral route to negative refraction," *Science*, vol. 306, pp. 1352–1355, 2004.

[14] D. L. Jaggard, A. R. Mickelson, and C. H. Papas, "On electromagnetic waves in chiral media," *Appl. Phys.*, vol. 18, pp. 211–216, 1979.

[15] A. V. Rogacheva, V. A. Fedotov, A. S. Schwanecke, and N. I. Zheludev, "Giant gyrotropy due to electromagnetic-field coupling in a bilayered chiral structure," *Phys. Rev. Letts.*, vol. 97, p. 177401, 2006.

[16] M. Silveirinha, "A metamaterial homogenization approach with application to the characterization of microstructured composites with negative parameters," *Phys. Rev. B*, vol. 75, p. 115104 (1–15), 2007.

[17] P. A. Belov, C. R. Simovski, and S. A. Tretyakov, "Example of bianisotropic electromagnetic crystals: The spiral medium," *Phys. Rev. E*, vol. 67, p. 056622, 2003.

[18] M. G. Silveirinha and C. A. Fernandes, "Homogenization of 3D-connected and non-connected wire metamaterials," *IEEE Trans. Microw. Theory Tech.*, vol. 53, no. 4, pp. 1418–1430, April 2005.

[19] M. G. Silveirinha and C. A. Fernandes, "Effective permittivity of metallic crystals: A periodic Green's function formulation," *Electromagnetics*, no. 8, pp. 647–663, 2003.

[20] L. D. Landau and E. M. Lifshitz, *Electrodynamics of Continuous Media, Course of Theoretical Physics*. The Netherlands: Elsevier Butterworth-Heinemann, 2004, vol. 8.

[21] A. N. Serdyukov, I. V. Semchenko, S. A. Tretyakov, and A. Sihvola, *Electromagnetics of Bi-Anisotropic Materials: Theory and Applications*. Amsterdam, The Netherlands: Gordon and Breach, 2001.

[22] P. A. Belov, R. Marques, S. I. Maslovski, I. S. Nefedov, M. Silveirinha, C. R. Simovski, and S. A. Tretyakov, "Strong spatial dispersion in wire media in the very large wavelength limit," *Phys. Rev. B*, vol. 67, p. 113103, 2003.

[23] M. Silveirinha, "Additional boundary condition for the wire medium," *IEEE Trans. Antennas Propag.*, vol. 54, p. 1766, 2006.

[24] M. G. Silveirinha and C. A. Fernandes, "A hybrid method for the efficient calculation of the band structure of 3D metallic crystals," *IEEE Trans. Microw. Theory Tech.*, vol. 52, no. 3, pp. 889–902, March 2004.

[25] W. Boothby, *An Introduction to Differentiable Manifolds and Riemannian Geometry*. New York: Academic Press, 1975.

Mário G. Silveirinha (S'99–M'03) received the "Licenciado" degree in electrical engineering from the University of Coimbra, Portugal, in 1998 and the Ph.D. degree in electrical and computer engineering from the Instituto Superior Técnico (IST), Technical University of Lisbon, Lisbon, Portugal, in 2003.

Since 2003, he has been an Assistant Professor at the University of Coimbra. His research interests include electromagnetic wave propagation in structured materials and homogenization theory.